Journal of Advanced Manufacturing Systems
Vol. 19, No. 4 (2020) 869–891

DOI: 10.1142/S0219686720500419

Optimization of A-TIG Welding Process Using Simulated Annealing Algorithm

Masoud Azadi Moghaddam

Department of Mechanical Engineering
Ferdowsi University of Mashhad
Mashhad, Iran
masoudazadi888@gmail.com

Farhad Kolahan*

Department of Mechanical Engineering
Ferdowsi University of Mashhad
Mashhad, Iran
kolahan@um.ac.ir

Flux-assisted tungsten inert gas welding process, also known as activated tungsten inert gas (A-TIG) welding, is extensively used in order to improve the performance of the conventional TIG welding process. In this study, the orthogonal array Taguchi (OA-Taguchi) method, regression modeling, analysis of variance (ANOVA) and simulated annealing (SA) algorithm have been used to model and optimize the process responses in A-TIG welding process. Welding current (I), welding speed (S) and welding gap (G) have been considered as process input variables for fabricating AISI316L austenitic stainless steel specimens. Depth of penetration (DOP) and weld bead width (WBW) have been taken into account as the process responses. In this study, SiO_2, nano-particle has been considered as an activating flux. To gather required data for modeling, statistical analysis and optimization purposes, OA-Taguchi based on the design of experiments (DOE) has been employed. Then the process responses have been measured and their corresponding signal-to-noise (S/N) ratio values have been calculated. Different regression equations have been applied to model the responses. Based on the ANOVA results, the most fitted models have been selected as an authentic representative of the process responses. Furthermore, the welding current has been determined as the most important variable affecting DOP and WBW with 68% and 88% contributions, respectively. Next, the SA algorithm has been used to optimize the developed models in such a way that WBW is minimized and DOP is maximized. Finally, experimental performance evaluation tests have been carried out, based on which it can be concluded that the proposed procedure is quite efficient (with less than 4% error) in modeling and optimization of the A-TIG welding process.

Keywords: Activated TIG welding process; OA-Taguchi method; regression modeling; analysis of variance; optimization; simulated annealing algorithm.

1. Introduction

Nowadays, gas tungsten arc welding (GTAW), also known as tungsten inert gas (TIG) welding, is one of the most extensively used welding processes for fabricating a

*Corresponding author.

wide variety of materials including stainless steels parts due to its good quality and surface finish. As the TIG welding process produces a shallow penetration, its application for fabricating the thick parts in a single pass has been restricted.[1–3] To tackle the problem of poor penetration in conventional TIG welding process, different procedures have been introduced among which pulsed current TIG (PCTIG) and activated TIG (A-TIG) welding processes are the most important ones.[6–14]

In order to obtain the maximum impact toughness properties of Titanium (Ti-6Al-4V) alloy welded parts in PCTIG welding, process variables have been optimized using a technique proposed by Balasubramanian *et al.*[6] Four important process variables, including peak and base current, pulse frequency, and pulse on time have been taken into account. DOE approach, regression modeling and statistical analysis have been used to design the experimental matrix and develop a mathematical model for predicting the process response (impact toughness). Then, the developed model has been optimized using the traditional Hooke and Jeeve's algorithm.

In the PCTIG welding process, fusion zone grain refinement is controlled by pulsed current variables (peak current, background current, pulse on time and frequency). A mathematical model has been developed by Balasubramanian *et al.*[7] to predict the corrosion rate of titanium alloy welded parts. Response surface methodology (RSM) has been employed to design the experimental matrix required for gathering information. Moreover, to attain the minimum corrosion rate in the weld fusion zone, the developed model has been optimized using a genetic algorithm (GA) and contour plots. The optimum variables to obtain minimum corrosion rate are as follows: 5.67 Hz of pulsing frequency, 35% for pulse on time, and 84.59 and 60 A of peak current and base current, respectively. Under these conditions, the lowest corrosion rate was found to be 0.007 mils/year.

A-TIG or flux-assisted TIG welding process is another extensively used technique to tackle the problem of poor penetration in the conventional TIG welding process. In the A-TIG welding process, a thin layer of activating flux is coated on the weld surface before the welding process begins. This process has been proposed by the Paton institute of electric in 1960.[4] A-TIG welding process has been effectively employed for welding of different materials, namely, aluminum, magnesium, titanium, stainless steel alloys (including austenite and austenite duplex), and also dissimilar metals.[9–11] Application of A-TIG welding process allowed steel parts (of around 10 mm) to be welded with single-pass welding without even using filler metal and edge preparation.[9]

To tackle the drawback of poor penetration in the TIG welding process of thick plates and pipes, the A-TIG welding process has been used by Kumar *et al.*[12] Based on the results, full penetration has been achieved using A-TIG welding process in comparison with conventional TIG welding process. Venkatesan *et al.*[13] reported that the A-TIG welding process eliminates edge preparation and reduces the number of welding passes required for accomplishing the fabricating process. Mechanical properties improvement and reduction of distortion were introduced as the main

assets of the A-TIG welding process by Chern *et al.*[14] Different fluxes (including oxide, chloride, and fluoride fluxes) have been employed by Tathgir *et al.*[15] in A-TIG welding process of stainless steel and low alloy parts to improve DOP. Based on the research results, using oxide fluxes results in the largest DOP in comparison with other ones. The effect of activating fluxes on mechanical and microstructural properties of magnesium alloy joints has been investigated by Qin *et al.*[16] Tensile strength and WBW of the A-TIG-welded AZ61/ZK60 joints illustrated strong dependence on the amount of TiO_2, which is used as the activating flux in A-TIG welding process. However, the inhomogeneity of the heat-affected zone (HAZ) near different base metals presented no significant effect on the mechanical properties of the welded joint. AISI 316 L austenitic stainless steel and P91 steel weldments have been fabricated by the A-TIG welding process in which thorough penetration of thick plates (8 mm) has been achieved in a single pass without edge preparation.[17] Results of conventional TIG and A-TIG welding processes revealed that hot cracking has been eliminated using the A-TIG welding process. Moreover, impact toughness has improved the ductility of the weld joints without significant loss of tensile strength. Effects of using activating fluxes (CeO_2 and MoO_3) on weld bead geometry, heat input, and angular distortion in the A-TIG welding process of P91 steel parts have been evaluated and compared with the conventional TIG welding process by Vidyarthy and Dwivedi.[18] Furthermore, microstructure, microhardness, tensile, and charpy impact tests have been taken into account. It was revealed that in the presence of activating fluxes, the heat input increases at the same welding input variables (welding current, welding speed and arc length). An increase of 200% and 300% in joint penetration was obtained using CeO_2 and MoO_3 fluxes, respectively. Based on the tensile strength tests, the A-TIG weldments revealed better results. However, the impact toughness of the A-TIG weldments was very low in comparison with the base metal.

There are different studies where the A-TIG welding process has been considered. Nonetheless, to the best of our knowledge, there is no published study in which modeling and optimization of DOP and WBW are considered using design of experiments (OA-Taguchi method) for designing experimental matrix, mathematical modeling (regression) for establishing the relationships between process input variables and process responses, statistical analysis (ANOVA) for determining the most fitted models and significant variables, and SA algorithm for optimization of process responses (DOP and WBW). Therefore, in this study, three process input variables (welding current (I), welding speed (S) and welding gap (G)) have been taken into account. Moreover, DOP and WBW have been considered as process responses. In the proposed approach, an experimental matrix has been designed based on the OA-Taguchi method. Regression modeling has been performed to establish the relations between process input variables and output responses. Then, in order to choose the most fitted derived equation from regression equations as the authentic representatives of the process, the ANOVA technique has been performed.

Furthermore, the significance of the process input variables and their corresponding percent contribution (e.g. 68% and 88% percent contribution reported for welding current affecting DOP and WBW respectively) on the process response measures has been determined based on the ANOVA results. Next, in order to maximize DOP and minimize WBW, the SA algorithm has been used. Based on the optimization results, the proposed procedure is quite efficient in modeling and optimization of the A-TIG welding process. The proposed approach has been performed on AISI316L austenitic stainless steel sheets, a widely used alloy in various industries including petrochemical, power plant, food industries and oil pipelines due to its superb mixture of strength and ductility and oxidation and corrosion resistance.

2. Experimental Setup and Equipment Used

In this study, a welding machine (DIGITIG 250 AC/DC, GAAM-Co, Iran) has been employed to conduct the experiments based on the OA-Taguchi experimental matrix (Fig. 1). Moreover, tungsten electrodes (with 2% Thorium) and argon shielding gas (with 99.7% purity) have been used.

Experiments have been conducted on AISI 316L austenitic stainless steel specimens with a dimension of $100 \times 50 \times 10$ (mm). The chemical composition of the material used (Table 1) has been determined using the XRF test (Fig. 2).

Prior to the welding process, 20 g of Nanosilicon dioxide (SiO_2) (+99%, 20–30 nm, amorphous) was mixed with 20 ml of carrier solvent (methanol) and mixed using a mechanical and an ultrasonic mixer until a paste-like flux attained (approximately 20 min). Then, the flux was coated on the specimen with a brush and dried before the welding begins. When the carrier solvent evaporated, the flux layer remained attached to the surface of the specimen (Fig. 3).

Fig. 1. TIG welding machine used for conducting the experiments.

Table 1. Chemical composition of material used (AISI316L).

Composition	Percentage (%)
Si	1.0
C	0.030
Cr	16.0–18.0
Mn	2.0
P	0.035
S	0.030
Ni	10.0–14.0
Mo	2.0-3.0

Fig. 2. Chemical composition determination using XRF test.

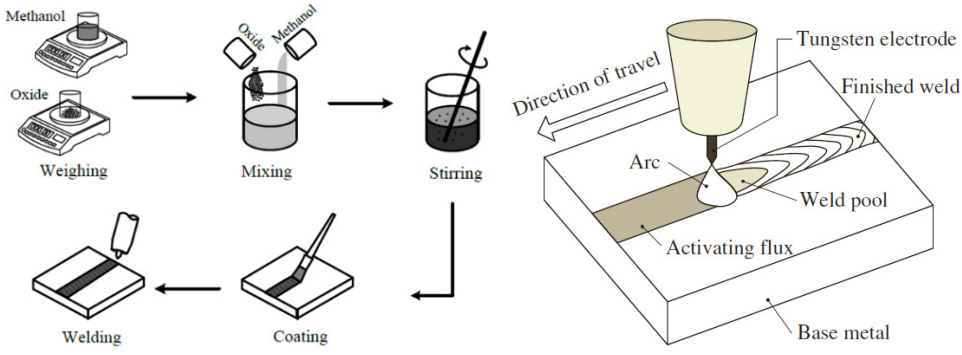

Fig. 3. Activated flux preparation and schematic diagram of A-TIG welding process.[16]

2.1. *A-TIG welding process input variables and their corresponding levels*

There are different A-TIG welding input variables among which welding current (I), welding speed (S) and welding gap (G) are the most significant ones.[1–3] Similarly, the

Table 2. A-TIG welding process input variables and their corresponding levels.

Process parameter	Welding gap (G)	Welding current (I)	Welding speed (S)
Unit	Mm	Amps	mm/sec
symbol	G	I	S
Interval	0.75–1.50	100-280	1.00-3.33
Level 1	0.75	100	1.00
Level 2	1.50	160	1.67
Level 3	—	220	2.67
Level 4	—	280	3.33

most important process responses include DOP and WBW. Feasible process input variables and their corresponding intervals of each have been determined based on the welding references, literature reviews and some preliminary tests (screening procedure). In the screening procedure, in order to determine the most important process input variables, they are considered at two levels. When the most important variables have been determined (ignoring the trivial ones) based on the experimental tests, the corresponding levels of the main variables chosen have been expanded.[8–15] In addition, the limitations of laboratory equipment may also indicate a certain number of levels for some of the process input variables. Table 2 lists the process input variables and their feasible intervals and levels.

2.2. *Design of experiments (DOE) approach*

When the main process input variables and their corresponding intervals and levels have been selected, an appropriate design matrix for conducting the experiments and data gathering purposes must be determined. To facilitate the identification of the influence of individual variables, establish the relationships between process input variables and output responses, and finally determine the optimal levels of process input variables in order to get the desired responses (e.g. maximum DOP and minimum WBW), DOE approach is used. one of the effective methods that can intensely reduce the number of experiments required for gathering necessary data is the OA-Taguchi method.[19,20] The OA-Taguchi method is widely used when the process input variables levels are unequal (unbalanced). Based on the number of input variables and their corresponding levels, a Taguchi's L_{32} design matrix has been chosen using MINITAB Software (Table 3).

2.3. *Experimental results*

To increase the accuracy, experiments have been conducted in random orders. After welding, two process responses (DOP and WBW) have been taken from each sample. Figure 4 displays a specimen welded under the same parameter levels for both conventional TIG and A-TIG welding process. As shown, A-TIG process results in smaller WBW and higher DOP.

Table 3. OA-Taguchi experimental matrix and measured responses and calculated S/N values.

No.	Welding gap	Welding current	Welding speed	Depth of Penetration (mm)	Weld bead width (mm)	S/N value for DOP	S/N value for WBW
1	0.75	100	1.00	3.25	4.42	23.5731	−29.7228
2	0.75	100	1.67	2.99	3.84	21.9055	−26.9094
3	0.75	100	2.67	2.28	3.95	16.4835	−27.4743
4	0.75	100	3.33	1.95	3.86	13.3566	−27.0133
5	0.75	160	1.00	5.48	6.26	34.0221	−36.6836
6	0.75	160	1.67	4.94	5.40	31.9473	−33.7280
7	0.75	160	2.67	2.79	6.31	20.5208	−36.8427
8	0.75	160	3.33	3.10	5.11	22.6280	−32.6240
9	0.75	220	1.00	7.83	10.69	41.1593	−47.3862
10	0.75	220	1.67	5.91	7.57	35.5329	−40.4839
11	0.75	220	2.67	4.56	6.28	30.3465	−36.7474
12	0.75	220	3.33	3.97	7.44	27.5753	−40.1374
13	0.75	280	1.00	9.06	11.84	44.0774	−49.4297
14	0.75	280	1.67	6.66	10.85	37.9224	−47.6833
15	0.75	280	2.67	5.63	7.87	34.5622	−41.2612
16	0.75	280	3.33	4.55	8.81	30.3025	−43.5177
17	1.50	100	1.00	3.08	5.23	22.4986	−33.0882
18	1.50	100	1.67	2.58	4.65	18.9558	−30.7373
19	1.50	100	2.67	2.37	4.05	17.2578	−27.9743
20	1.50	100	3.33	2.02	4.16	14.0620	−28.5103
21	1.50	160	1.00	5.42	7.12	33.8019	−39.2582
22	1.50	160	1.67	4.27	6.52	29.0323	−37.4975
23	1.50	160	2.67	3.38	6.19	24.3575	−36.4587
24	1.50	160	3.33	3.26	6.15	23.6345	−36.3290
25	1.50	220	1.00	8.04	9.36	41.6886	−44.7289
26	1.50	220	1.67	5.83	8.29	35.2603	−42.3010
27	1.50	220	2.67	4.60	8.14	30.5211	−41.9358
28	1.50	220	3.33	4.23	7.68	28.8440	−40.7724
29	1.50	280	1.00	10.00	11.97	46.0517	−49.6481
30	1.50	280	1.67	6.67	11.12	37.9524	−48.1749
31	1.50	280	2.67	5.27	10.25	33.2406	−46.5456
32	1.50	280	3.33	5.04	9.69	32.3481	−45.4219

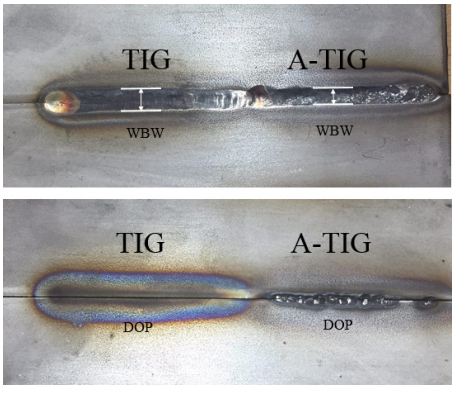

Fig. 4. Output characteristics comparison of a welded sample using the C-TIG and A-TIG process.

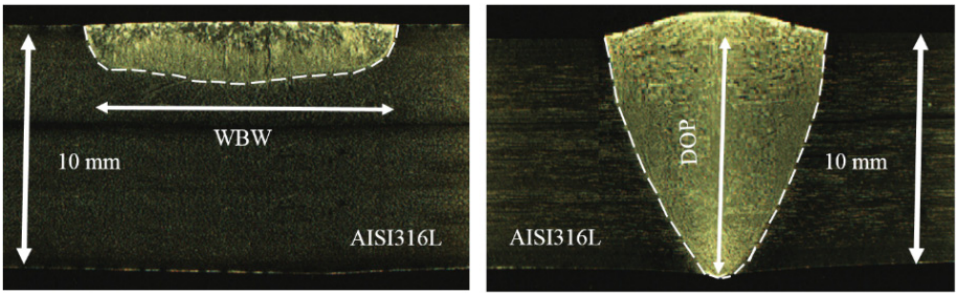

Fig. 5. Comparison of TIG and A-TIG weldments cross-sections.

For measuring DOP and WBW, on each sample, two transverse cross-sections were made. Next, to clearly show DOP and WBW, the cut faces were smoothly polished and etched (Fig. 5).

Then, for taking images, an optical microscope has been used. To determine samples DOP and WBW, images were consequently processed by MIP (microstructural image processing) software. The average of two measurements for each sample was reported in Table 3.

3. Signal-to-Noise (S/N) Ratio

To study the whole process input variables space with small numbers of experiments, the Taguchi method has been extensively used. The Taguchi method also uses the signal-to-noise (S/N) ratio as performance measure to optimize the process input variables for desired output responses. To compute the deviation between the experimental and desired values, a loss function is introduced. Then, the loss function is transformed into S/N ratio. The S/N ratio calculation may be decided as "smallest is the best, (SB)" (used for measures in which the smallest amount is desired, e.g. WBW) or "largest is the best, (LB)" (used for measures where the largest amount is desired, e.g. DOP) based on the determined responses, as given in the following equations[21]:

$$\textbf{LB} : S/N(\varphi) = -10 \ \log\left(\frac{1}{n}\sum_{K=1}^{n}\frac{1}{x_K^2}\right), \tag{3.1}$$

$$\textbf{SB} : S/N(\eta) = -10 \ \log\left(\frac{1}{n}\sum_{K=1}^{n}x_K^2\right), \tag{3.2}$$

where the number of iteration in a trial is shown as n (in this study, $n = 1$), and x_K is the jth measured value in a run. Therefore, as the largest DOP and the smallest WBW values are desired, Eqs. (3.1) and (3.2) are considered to calculate S/N ratio values, respectively. The experimental results of 32 experiments (fifth and sixth columns) and their corresponding S/N ratio values (seventh and eighth columns) based on the OA-Taguchi method are reported in Table 3.

4. Regression Modeling

Regression modeling is a statistical procedure using which the relationships between process input variables and output responses are estimated. To carry out the regression modeling and corresponding analysis (ANOVA), the following steps must be taken into account.[22]

First, input variables and output responses of the process under consideration are identified. Then, intervals of process input variables are determined using literature survey, preliminary experiments, and screening methods. Selection of a DOE matrix based on the process input variables and their corresponding levels (such as full factorial and fractional factorial designs) is the next step. Next, the experiments are conducted and the required data are also collected. Then the process response equations are driven by developing mathematical models and conducting a significance test using ANOVA (F-test and P-test). Finally, the most fitted models are selected as the representatives of the process responses [22].

The first three columns of Table 3 are the process input variables levels. The next two columns are the measured DOP and WBW values based on the conducted experiments in each row. The last two columns are the calculated S/N ratio values for the measured responses. Any of the above output is a function of process variables that are expressed by linear, second-order/curvilinear or modified second-order (with elimination of trivial parameters) and logarithmic functions, as stated in the following equations[22]:

$$Y_1 = a_0 + a_1 B + a_2 C + a_3 D, \tag{4.1}$$

$$Y_2 = a_0 + a_1 B + a_2 C + a_3 D + a_{11} BB + a_{22} CC + a_{33} DD + a_{12} BC + a_{13} BD + a_{23} CD, \tag{4.2}$$

$$Y_3 = a_0 \times B^{a1} \times C^{a2} \times D^{a3}, \tag{4.3}$$

where regression constants are shown with a_0, a_1, a_2 and a_3 and are to be predicted. Furthermore, B, C and D are input variables (I, S, and G) and Y_1, Y_2 and Y_3 are the output responses (S/N ratio values for DOP and WBW). Based on the calculated S/N ratios for DOP and WBW values given in Table 3, the regression equations are developed using MINITAB software. Models representing the relationship between process input variables and output responses could be stated in the following equations.

4.1. *Linear models*

$$\mathrm{S/N(WBW)} = -19.9 - 2.64 \times G - 0.166 \times I + 7.08 \times S + 0.000181 \times (I \times I) - 1.21 \times (S \times S), \tag{4.4}$$

$$\mathrm{S/N(DOP)} = 9.28 + 0.276 \times I - 9.07 \times S - 0.000402 \times (I \times I) + 1.32 \times (S \times S) - 0.00906 \times (I \times S). \tag{4.5}$$

4.2. *Logarithmic models*

$$\mathrm{S/N(WBW)} = e^{-1.69} \times G^{0.0807} \times I^{0.461} \times S^{-0.0965}, \tag{4.6}$$

$$\mathrm{S/N(DOP)} = e^{-3.05} \times I^{0.697} \times S^{-0.347}. \tag{4.7}$$

4.3. *Curvilinear models*

$$\mathrm{S/N(WBW)} = -20.9 - 2.64 \times G - 0.0970 \times I + 1.85 \times S, \tag{4.8}$$

$$\mathrm{S/N(DOP)} = 20.6 + 0.103 \times I - 5.07 \times S. \tag{4.9}$$

5. Performing Analysis of Variance (ANOVA)

To determine how well a model fits the experimental values and represent the authentic process under study, ANOVA is performed.[21] ANOVA procedure within 95% of confidence level has been employed to check the adequacy of the proposed models (Table 4).[21] Obviously, the second-order model (with the elimination of trivial variables) for DOP and logarithmic model for WBW are the superior models based on the required confidence level (Pr), the correlation factor (R^2) and the adjusted correlation factor (R^2-adj). Moreover, to examine the prediction ability of the proposed models, some extra experiments besides the predetermined experimental matrix (OA-Taguchi) have been conducted based on which the ANOVA results have been confirmed. Thus, these superior models were considered as the best authentic representatives of the A-TIG welding process responses in this study and the objective functions of the SA algorithm for optimization purposes.

The residual plots for DOP and WBW are shown in Figs. 6 and 7, respectively. These figures demonstrate a good conformability of the developed model to the real process (normal probability plot). Moreover, histogram plots show the normal distribution of the residuals. Based on the residual-fitted value plots, there is no pattern to be followed by the residuals. Furthermore, the order of observation versus residuals shows that the residual changes are accidental.

Table 4. ANOVA results of different models for the A-TIG welding process responses.

Model	Variable	R^2	R^2 (adj)	$F-$value	$\Pr > F$
Linear	DOP	94.0%	93.5%	225.31	< 0.0001
logarithmic	DOP	95.7%	95.4%	319.60	< 0.0001
Second-order	**DOP**	**98.0%**	**97.6%**	**249.28**	$<$ **0**.0001
Linear	WBW	94.4%	93.8%	156.73	< 0.0001
logarithmic	**WBW**	**96.4%**	**96.0%**	**246.62**	< 0.0001
Second-order	WBW	96.2%	95.4%	130.16	< 0.0001

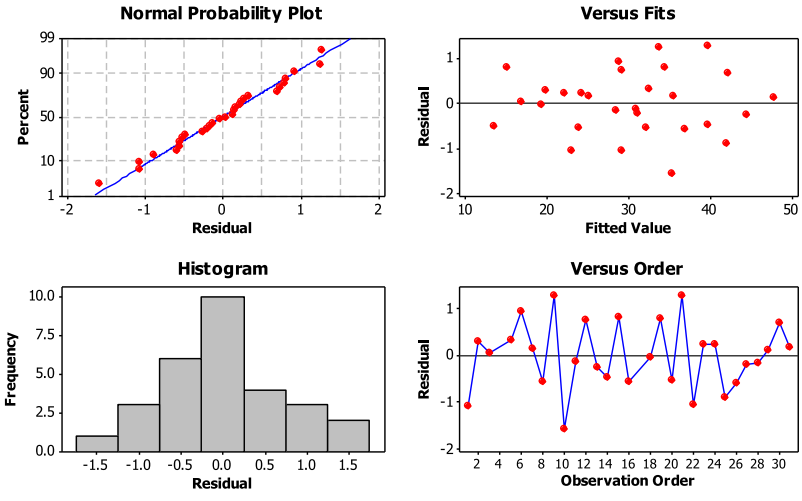

Fig. 6. Residual plot for depth of penetration (DOP)

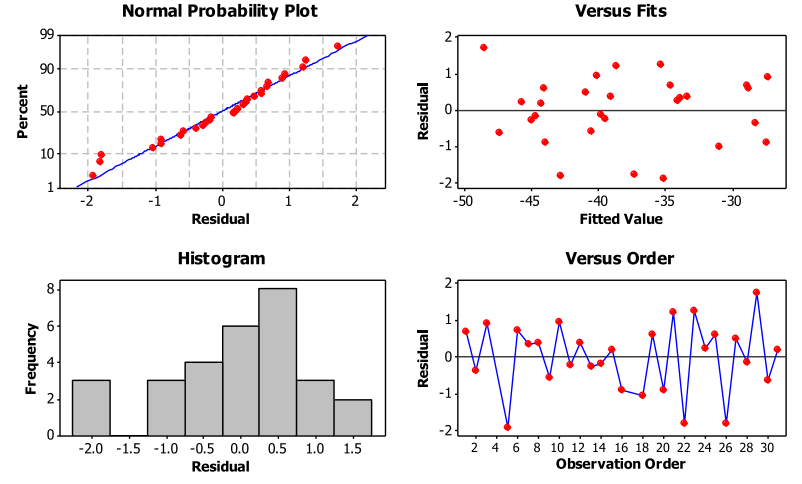

Fig. 7. Residual plot for weld bead width (WBW).

Detailed results of ANOVA are shown in Tables 5 and 6. Large F-value illustrates that the variation of the process variables makes a big change in the performance of the process responses. In this study, to evaluate process variables significance, a 95% confidence level has been considered. Therefore, F-values of A-TIG process variables were compared with the appropriate values from the confidence table, $F_{\alpha,v1,v2}$; where the risk, degrees of freedom associated with numerator and denominator illustrated in Tables 5 and 6 are shown by α, v_1 and v_2, respectively.[21] Within a confidence level of 95%, ANOVA results show that welding current, welding speed and welding gap are, respectively, the most important process variables affecting DOP and WBW.

Table 5. Result of ANOVA for S/N ratio of weld bead width (WBW).

Welding parameters	Degree of freedom (Dof)	Sum of square (SS_j)	Mean Square	*F*-Value	Percent contribution (%)
G	1	31.48	31.48	12.70	2
I	3	1369.90	456.63	184.26*	88
S	3	103.18	34.39	13.88*	7
Error	24	59.48	2.48	—	3
Total	31	1564.04	—	—	100
Significant Parameter *					

Table 6. Result of ANOVA for S/N ratio of the depth of penetration (DOP).

Welding parameters	Degree of freedom (Dof)	Sum of square (SS_j)	Mean Square	F-Value	Percent contribution (%)
G	1	0.40	0.40	0.17	1
I	3	1605.2	535.09	226.40*	68
S	3	677.60	225.87	95.57*	29
Error	24	56.72	2.36	—	2
Total	31	2340.00	—	—	100
Significant Parameter *					

The percent contribution of each process variable provided by ANOVA results using Eq. (5.1).[20] The percent contributions of the A-TIG welding process variables are shown in Figs. 8 and 9.

$$\mathrm{P}_i(\%) = \frac{\mathrm{SS}_i - (\mathrm{DOF}_i \times \mathrm{MS}_{\mathrm{error}})}{\mathrm{Total\ \ Sum\ \ of\ \ Squre}}, \tag{5.1}$$

where P_i is the contribution percentage of each variable under consideration, SS_i is the sum of square, DOF_i is the degree of freedom of ith factor, and $\mathrm{MS}_{\mathrm{error}}$ is the mean sum of square of error.[19]

According to Table 5, welding current at 88%, welding speed at 7%, and the welding gap at 2% are the most important variables affecting WBW.

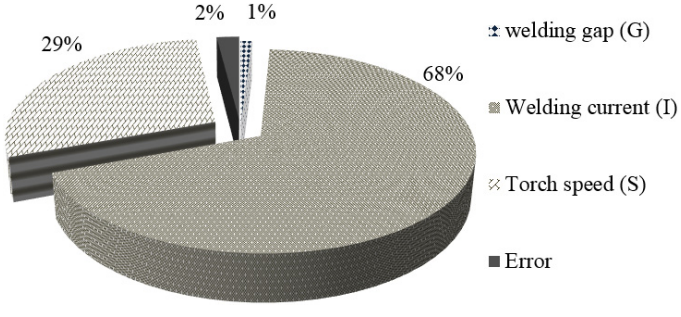

Fig. 8. Percent contributions of welding variables to the DOP.

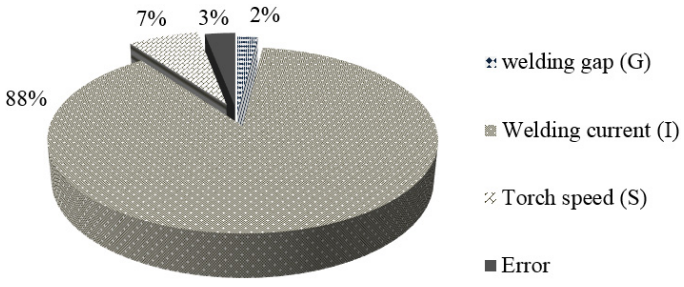

Fig. 9. Percent contributions of welding variables to the WBW.

By the same token, welding current is the major variable affecting DOP at 68% followed by welding speed and welding gap at 29% and 1% contribution, respectively. The rest (2%) is due to error and uncontrollable variables based on the nature of the process and the equipment used is acceptable (Table 6).

Figure 10 illustrates the interaction effect of process variables (welding current and speed) for DOP. Moreover, based on the ANOVA results, the welding gap has a trivial effect on the process responses (DOP and WBW), therefore, it has been considered at a fixed value. As illustrated, by increasing welding speed, the DOP decreases. Similarly, by increasing the welding current, the DOP increases. By the same token, Fig. 11 shows the interaction effect of process variables (welding current and speed) for WBW. As illustrated, by increasing welding current, WBW increases. Likewise, by increasing welding speed, the WBW decreases.

Interaction plot in Fig. 12 represents that WBW increases with higher welding current. As the same token, the lowest WBW reached at the highest speed. It is also observed that the interaction of the welding speed and welding gap has the least influence on WBW.

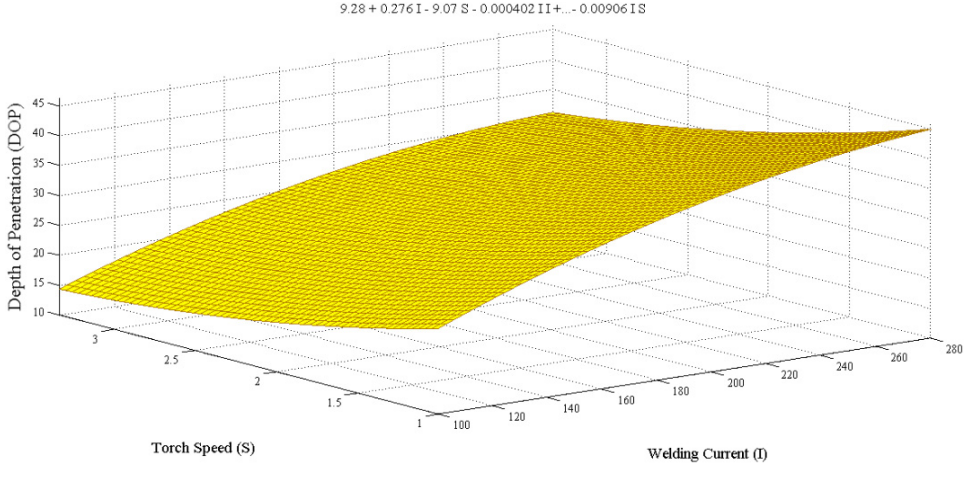

Fig. 10. Interaction of A-TIG welding process parameters for DOP.

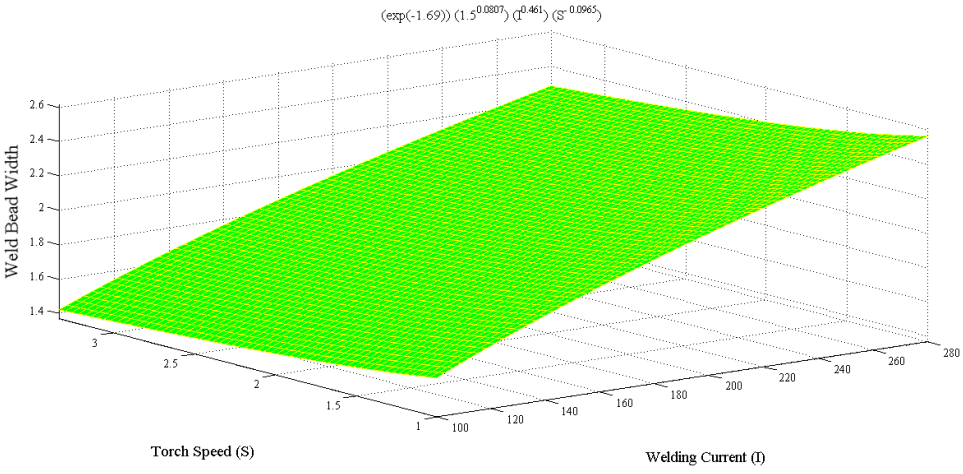

Fig. 11. Interaction of A-TIG welding process parameters for WBW.

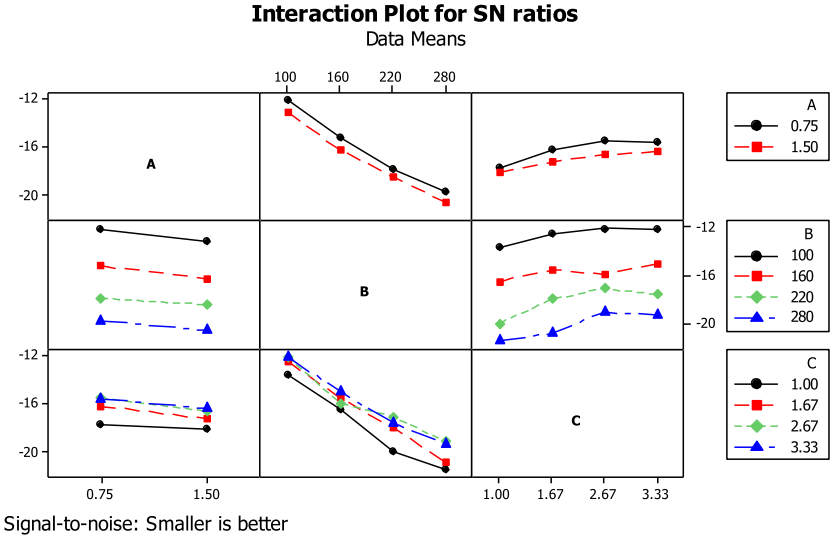

Fig. 12. Interaction plot of WBW for L32 OA-Taguchi method.

6. Optimization Procedure

6.1. *Taguchi-based optimization method*

To define the effect of each process input variables on the output responses, the mean of S/N ratio values for each test containing this variable in the desired level are calculated. Moreover, the calculated means for each level of input variable are compared and the level at which the highest value belongs is considered as the desired level to optimize the process responses.[20] For example, the mean effect of

Table 7. Response (mean) of S/N values for depth of penetration.

Symbol	Level 1	Level 2	Level 3	Level 4
G	29.119	***29.344***	—	—
I	18.512	27.493	33.866	***37.057***
S	***35.859***	31.064	25.911	24.094

Table 8. Response (mean) of S/N values for weld bead width.

Symbol	Level 1	Level 2	Level 3	Level 4
G	***−37.353***	−39.3364	—	—
I	***−28.929***	−36.1777	−41.812	−46.460
S	−41.243	−38.439	−36.905	***−36.791***

welding speed at level 1 is calculated from averaging test runs number 1, 2 up to 16. Along these lines, the mean effects of variables are computed and listed in Tables 7 and 8. Since the highest S/N mean value is favorable, with respect to the data in Table 7, the optimal set of variables for optimization of DOP is: G at level 2, I at level 4 and S at level 1, i.e. (G2 I4 S1). Similarly, the optimal set of variables for optimization of WBW is: G at level 1, I at level 1 and S at level 4, i.e. (G1I1 S4) based on results of Table 8. Moreover, Figs. 13 and 14 also illustrate the optimum variables setting in order to achieve the maximum DOP and minimum WBW.

As the S/N method in optimization procedure could only determine the best set of process variable levels from the predetermined ones in the design matrix used (Table 2), using heuristic algorithms would help to interpolate the answer space in order to find the best solution which may not be one of the determined levels

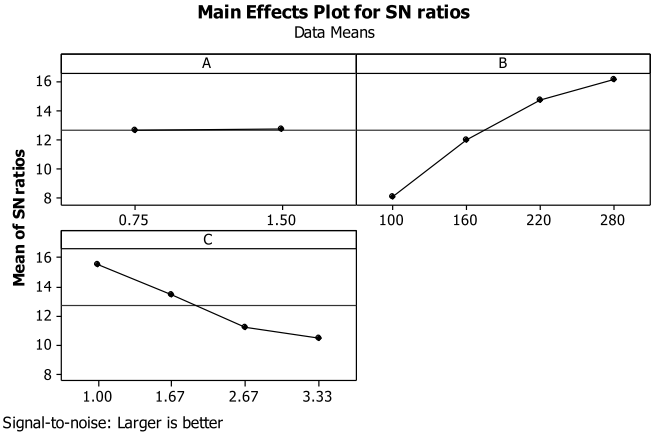

Fig. 13. The effect of A-TIG input process variables on the signal to noise (S/N) values of DOP.

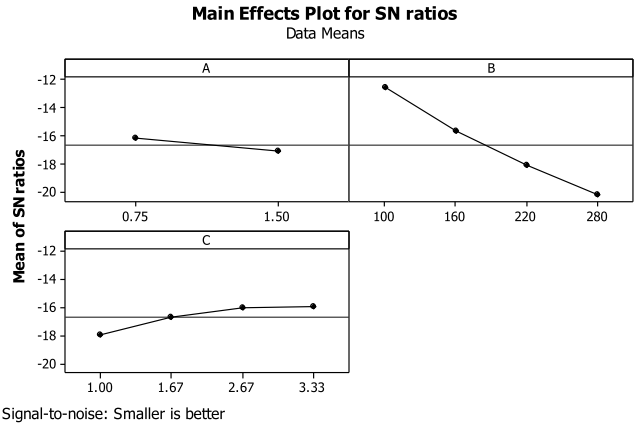

Fig. 14. The effect of A-TIG input process variables on the signal to noise (S/N) values of WBW.

considered in Table 2. In this study, the most fitted models are selected as a representative of the process responses and considered as the objective functions for the heuristic algorithm (SA).

7. Simulated Annealing Algorithm

Most of the heuristic algorithms have been proposed based on the physical phenomena, among which one of the most extensively used is the simulated annealing (SA) algorithm. SA is reminiscent of the physical annealing process in metalwork and effectively used in optimization problems.[29] In the annealing process, metals are heated up to a specific temperature. Therefore, at this temperature, all molecules of the metal are in intense random motion. Then, the metal is slowly cooled down. All molecules rearrange themselves and tend toward a low energy state. As the cooling process is carried out appropriately slow, lower and lower energy states until the lowest energy state is reached are obtained. Similarly, in the A-TIG welding process, an energy function (objective function) is created which is minimized. The lowest energy level gives the optimized value of A-TIG welding process variables. Recently, the SA algorithm has developed as a leading tool for complex optimization problems.[23,24]

The SA algorithm mechanism is defined as follows:

First, an initial random solution (C_0) within the acceptable answer space is generated. Then, a movement from the current solution is made and objective function of new solution (C_1) is calculated and compared with the current one ($\Delta C = C_{1\_}C_0$). Either, it has a better value or the probability function implemented in the SA algorithm has a higher value than a randomly generated number between 0 and 1, a movement is made to the new solution. Equation (7.1) gives the following probability of accepting a new solution[24]:

$$P = \mathrm{Exp}\left(-\frac{\Delta C}{T_k}\right), \tag{7.1}$$

where the temperature parameter plays a similar role as the temperature in the physical annealing process and is shown by T_k.[23] In our problem, temperature reduction has been done using the following equation:

$$T_{k+1} = \alpha \times T_k \quad k = 0, 1, \ldots \quad \text{and} \quad 0.9 \leq \alpha < 1, \tag{7.2}$$

where the current and former temperatures are shown by T_{k+1} and T_k, respectively. Parameter α presents the cooling rate. Consequently, at the initial iterations of SA,

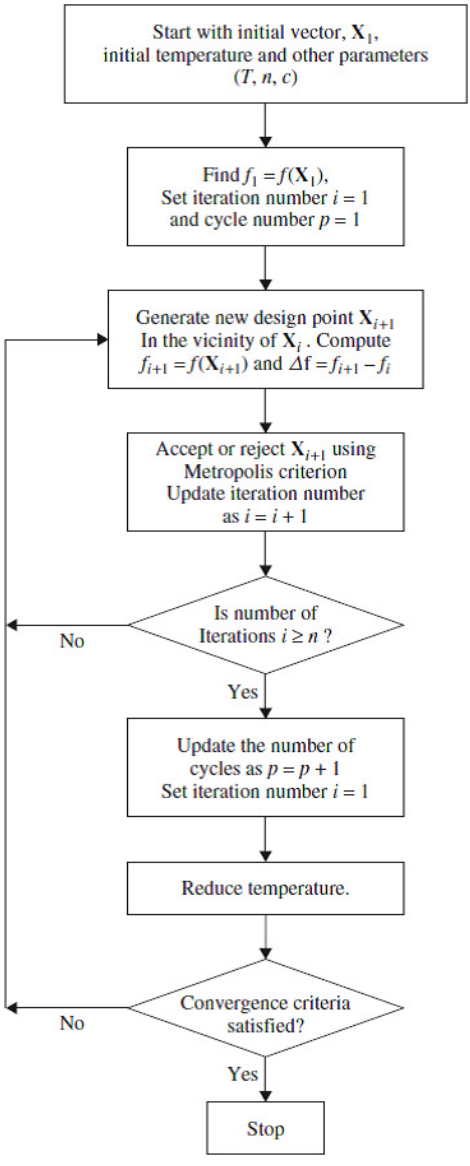

Fig. 15. Schematic illustration of simulated annealing algorithm procedure.[24]

Table 9. Results of optimization based on the Taguchi and SA algorithm methods.

Parameters	Set of Parameters				Predicted S/N value	Experimental S/N value	Error (%)	Improvement of S/N value
	Input parameters	G	I	S				
Best set of parameters in L_{32} experiments	Setting Levels for optimized DOP	1.50	280	1.00	46.0517	46.0517	—	—
	Setting Level for optimized WBW	0.75	100	1.67	−26.9094	−26.9094	—	—
Taguchi optimization	Setting Levels for optimized DOP	1.50	280	1.00	46.0517	43.1270	6.3	2.9247
	Setting Level for optimized WBW	0.75	100	3.33	−25.0133	−28.8160	6.7	3.8027
Simulated annealing algorithm optimization	Setting Levels for optimized DOP	1.50	280	1.036	49.6648	48.2256	2.9	2.1739
	Setting Level for optimized WBW	1.00	153	2.85	−21.7038	−20.9952	3.3	5.9138

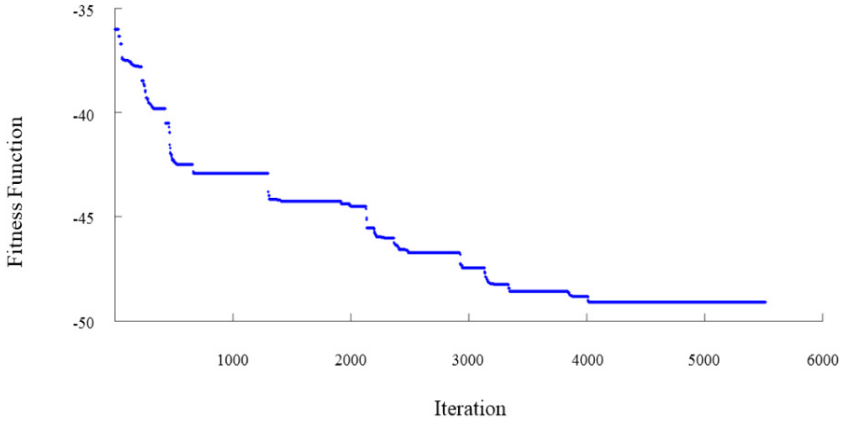

Fig. 16. Simulated annealing algorithm convergence for DOP optimization.

most of the worsening moves may be accepted due to higher temperatures, but at the end of the procedure only improving ones are likely to be allowed. This can help the process to avoid getting trapped in a local minimum and jump out of it. After a certain number of iterations, a predetermined run time, or a number of iterations in which no development is detected, the algorithm may be terminated. Flowchart of SA algorithm for A-TIG welding process optimization is shown in Fig. 15. Table 9 indicates that for maximum DOP, the welding current and welding gap should be considered at their highest levels. Likewise, for achieving lower WBW, welding current and welding gap should be approximately set at their lower ranges. The convergence of SA algorithm for DOP response is shown in Fig. 16.

8. Technical Discussion

In the welding process, the size and shape of the weld bead have been determined based on the molten metal fluid flow mode in the welding pool. Generally, the welding arc heat and plasma channel shape have a significant influence on the fluid flow and the weld pool surface tension.[25] There are two phenomena (reversal of Marangoni convention and arc constriction) based on which the shape and size of the weld pool are determined.

At the weld pool center, surface tension (σ) is lesser than the outer edges, consequently, the surface tension gradient is negative ($(\partial\sigma/\partial T) < 0$). Thus, the Marangoni convection occurs from the center towards weld edges direction, which results in a wide and shallow weld pool. During the A-TIG welding process, the top surface of the weldments is covered with paste-like flux. The presence of oxygen, as a surface-active element in molten metal reverses the Marangoni convection, changes the direction of surface tension gradient from the boundary of the weld pool towards the center; therefore, the surface tension gradient becomes positive ($(\partial\sigma/\partial T) > 0$). This phenomenon results in an increase in penetration and reduction in welding width.

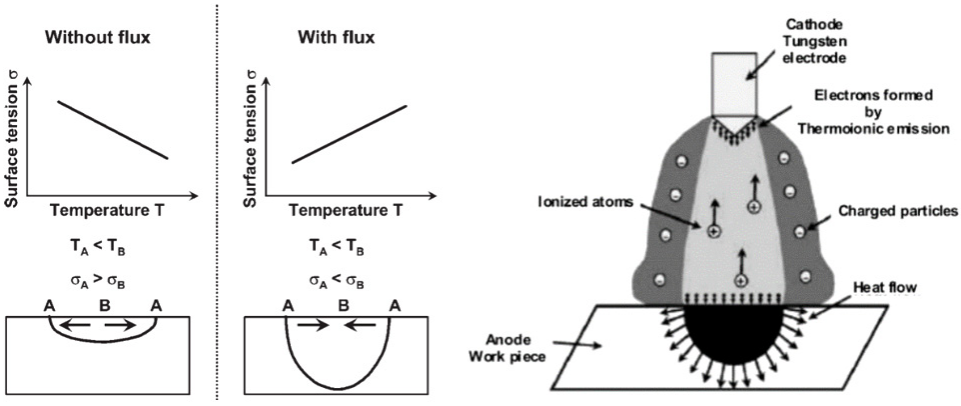

Fig. 17. Reversal of Marangoni convection and arc constriction schematic illustrations.

Types of fluxes and their compositions significantly determine the arc constriction phenomenon. The paste-like flux covered on the surface of the weldments gets vaporized partially. The remaining flux gets mixed with the molten metal pool when the welding arc passes over the layer deposited. The electrons in the cooler outer areas, where they have small energy in a fragile electric field, have been captured by vaporized flux. Nevertheless, in the central region of arc, due to the high temperature, presence of the robust electric field, and high energy, electrons ionization would dominate. The current flow in the central region of the arc column is restricted. Therefore, an increased current density at the anode center is obtained. In Fig. 17, the schematic illustration of the phenomena has been shown.[26,27]

The delta-ferrite content of AISI316L stainless steel is 1.2 ferrite number (FN), whereas this value is increased to 6.1 FN after the TIG welding process conducted due to solidification as delta-ferrite phase.[24] During the welding process, the cooling rate of the weld metal is rapid enough that the phase transformation of delta-ferrite to austenite is not completed. Consequently, solidification accomplished more delta-ferrite retained in the weld metal. On the other hand, when using oxide fluxes, the delta-ferrite content in the weld metal increased to 7.0–7.6 FN due to heat input during the A-TIG welding process. It is also found that the arc voltage increases when activating fluxes are used. Since the calculated heat input is proportional to the measured arc voltage, applied activating fluxes have the positive effect of increasing heat input. Therefore, this higher heat input can increase the peak temperature, and consequently, more delta-ferrite forms in the weld metal. All cases exhibited an austenite microstructure matrix and vermicular delta-ferrite morphology typical of this class of material.[28,29]

The crystal structure of austenite is cubic face-centered (FCC), whereas the crystal structure of delta ferrite is body-centered cubic (BCC). The BCC structure has a higher mechanical strength in comparison with the FCC structure. When the A-TIG welding process is used, the delta-ferrite content in the weld metals is increased and has a beneficial effect in increasing the hardness of AISI316L weldments.[30]

In the A-TIG welding process based on the reversal of Marangoni convection and arc constriction phenomena, the WBW will be reduced, therefore, the heat affected zone (HAZ) will be smaller in comparison to the conventional TIG welding process. Moreover, rapid solidification results in smaller grain size. Smaller HAZ and grain size will be ended in higher corrosion resistance in this process.

9. Conclusion

Proper selection of process variables levels positively affects the quality of weldments in welding processes. In this study, the problem of poor penetration and wide weld bead width in the conventional TIG welding process has been addressed using activating fluxes. Moreover, modeling and optimization of these responses in the welding of AISI316L austenite stainless steel parts have been performed. First, A-TIG welding experimental tests have been conducted based on experimental data gathered as per the L_{32} OA-Taguchi method. Then, DOP and WBW values have been measured using MIP software. Then, S/N values have been calculated based on the desired responses. Regression modeling has been used to formulate the process responses (DOP and WBW) as a function of input variables (welding current, welding speed and welding gap). Next, ANOVA has been used in order to determine the most fitted models as an authentic representative of the process responses. Furthermore, significant variables and their corresponding percent contribution on each process response have been determined using ANOVA. Results showed that welding current is the most important variable affecting DOP and WBW at 68% and 88% contribution, respectively. Furthermore, the minor effect belongs to the welding gap. Next, in order to optimize the process responses, the SA algorithm and Taguchi method (signal to noise analysis) have been used. Furthermore, the results of optimization procedures have been confirmed using experimental tests. Based on the results, the proposed method can accurately (with less than 4% error) simulate and optimize the A-TIG welding process.

References

1. H. Y. Huang, S. W. Shyu, K. H. Tseng and C. P. Chou, Evaluation of TIG flux welding on the characteristics of stainless steel, *J. Sci Technol Weld Join* **10** (2005) 566–573, doi: 10.1179/174329305X48329.
2. S. W. Shyu, H. Y. Huang, K. H. Tseng and C. P. Chou, Study of the performance of stainless steel A-TIG welds, *Mater. Eng. Perform.* **17** (2008) 197–201, doi: 10.1007/s11665-007-9139-7.
3. H. Fujii, T. Sato, S. P. LU and K. Nogi, Development of an advanced A-TIG (AA-TIG) welding method by control of Marangoni convection, *Mater. Sci. Eng. A* **495** (2008) 296–303, doi: 10.1016/j.msea.2007.10.116.
4. S. Z. Li, J. Shen, Z. M. Cao, L. Z. Wang and N. Xu, Effects of mix activated fluxes coating on microstructures and mechanical properties of tungsten inert gas welded AZ31 magnesium alloy joints, *Sci. Technol. Welding Joining* **17** (2012) 467–475, doi: 10.1179/1362171812Y.0000000037.

5. S. A. Kumar and P. Sathiya, Experimental investigation of the A-TIG welding process of incoloy 800H, *Mater. Manuf. Process.* **30** (2015) 1154–1159, doi: 10.1080/10426914.2015.1019092.
6. M. Balasubramanian, V. Jayabalan and V. Balasubramanian, Optimizing the pulsed current GTAW parameters to attain maximum impact toughness, *Mater. Manuf. Process.* **23** (2008) 69–73, doi: 10.1080/10426910701524584.
7. M. Balasubramanian, V. Jayabalan and V. Balasubramanian, Optimizing pulsed current parameters to minimize corrosion rate in gas tungsten arc welded titanium alloy, *Int. J. Adv. Manuf. Technol.* **39** (2008) 474–481, doi: 10.1007/s00170-007-12333.
8. K. H. Dhandha and V. J. Badheka, Effect of activating fluxes on weld bead morphology of P91 steel bead-on-plate welds by flux assisted tungsten inert gas welding process, *Mater. Manuf. Process.* **17** (2015) 48–57, doi: 10.1016/j.jmapro.2014.10.004.
9. R. S. Vidyarthy, A. Kulkarni and D. K. Dwivedi, Study of microstructure and mechanical property relationships of A-TIG welded P91-316L dissimilar steel joint, *Mater. Sci. Eng. A* **695** (2017) 249–257, doi: 10.1016/j.msea.2017.04.038.
10. K. D. Ramkumar, V. Varma, M. Prasad and N. D. Rajan, Effect of activated flux on penetration depth, microstructure and mechanical properties of Ti-6Al-4V TIG welds, *J. Mater. Process. Tech.* **261** (2018) 233–241, doi: 10.1016/j.jmatprotec.2018.06.024.
11. Y. Zou, R. Ueji and H. Fujii, Mechanical properties of advanced active-TIG welded duplex stainless steel and ferrite steel, *Mater. Sci. Eng. A* **620** (2015) 140–148, doi: 10.1016/j.msea.2014.10.006.
12. V. Kumar, Investigation of the A-TIG mechanism and the productivity benefits in TIG welding, *Fifteenth Int. Conf. Joining Mater.* **25** (2009) 1–11.
13. G. Venkatesan, V. Muthupandi and J. Justine, Activated TIG welding of AISI 304L using mono- and tri-component fluxes, *Int. J. Adv. Manuf. Technol.* **93** (2017) 329–336, doi: 10.1007/s00170-016-9002-9.
14. T. S. Chern, Study of the characteristics of duplex stainless steel activated tungsten inert gas welds, *Mater. Des.* **32** (2011) 255–263, doi: 10.1016/j.matdes.2010.05.056.
15. S. Tathgir and A. Bhattacharya, Activated-TIG welding of different steels: Influence of various flux and shielding gas, *Mater. Manuf. Process.* **31** (2015) 335–342, doi: 1080/10426914.2015.1037914.
16. B. Qin, F. C. Yin, C. Z. Zeng, J. C. Xie and J. Shen, Microstructure and mechanical properties of TIG/A-TIG welded AZ61/ZK60 magnesium alloy joints, *Trans. Nonferrous Metals Soc. China* **29** (2019) 1864–1872, doi: 10.1016/S1003-6326(19)65094-6.
17. A. Kulkarni, D. K. Dwivedi and M. Vasudevan, Dissimilar metal welding of P91 steel-AISI 316L SS with Incoloy 800 and Inconel 600 interlayers by using activated TIG welding process and its effect on the microstructure and mechanical properties, *J. Mater. Process. Technol.* **274** (2019) 116–128, doi: 10.1016/j.jmatprotec.2019.116280.
18. R. S. Vidyarthy and D. K. Dwivedi, Microstructural and mechanical properties assessment of the P91 A-TIG weld joints, *J. Manuf. Process.* **31** (2018) 523–535, doi: 10.1016/j.jmapro.2017.12.012.
19. F. Kolahan and M. Azadi Moghaddam, The use of Taguchi method with grey relational analysis to optimize the EDM process parameters with multiple quality characteristics, *Sci. Iran. B* **22** (2015) 530–538.
20. M. Azadi Moghaddam and F. Kolahan, Application of orthogonal array technique and particle swarm optimization approach in surface roughness modification when face milling AISI1045 steel parts, *J. Ind. Eng. Int.* **12** (2016) 199–209, doi: 10.1007/s40092-015-0137-3.
21. D. Vishnu, R. I. Asal, T. Patel and B. Alok, Optimization of process parameters of EDM using ANOVA method, *Int. J. Eng. Res. Appl.* **3** (2013) 1119–1125.

22. M. Vishwakarma and V. V. K. Parashar, Regression analysis and optimization of material removal rate on electric discharge machine for EN-19 alloy steel, *Int. J. Sci. Res. Pub.* **2** (2012) 167–175.
23. Y. Hu, Y. Shi, K. Sun and X. Shen, Microstructure evolution and mechanical performance of underwater local dry welded DSS metals at various simulated water depths, *J. Mater. Process. Technol.* **264** (2019) 366–376, doi: 10.1016/j.jmatprotec.2018.09.023.
24. B. Varbai, T. Pickle and K. Májlinger, Effect of heat input and role of nitrogen on the phase evolution of 2205 duplex stainless steel weldment, *Int. J. Pressure Vessels Piping* **176** (2019) 113–124.
25. M. Moradi, M. Ghoreishi and A. Khorram, Process and outcome comparison between laser, tungsten inert gas (TIG) and laser-TIG hybrid welding, *Lasers Eng.* **39** (2018) 379–391.
26. R. Pamnani, M. Vasudevan, T. Jayakumar and P. Vasantharaja, Development of activated flux, optimization of welding parameters and characterization of weld joint for DMR-249A shipbuilding steel, *Trans. Indian Inst. Met.* **70** (2017), doi: 10.1007/s12666-016-0857-0.
27. K. H. Tseng and C. Y. Hsu, Performance of activated TIG process in austenitic stainless steel welds, *J. Mater. Process. Technol.* **211** (2011) 503–512, doi: 10.1016/j.jmatprotec.2010.11.003.
28. K. H. Tseng, Development and application of oxide-based flux powder for tungsten inert gas welding of austenitic stainless steels, *Powder Technol.* **233** (2013) 72–90, doi: 10.1016/j.powtec.2012.08.038.
29. B. Arivazhagan and M. Vasudevan, A comparative study on the effect of GTAW processes on the microstructure and mechanical properties of P91 steel weld joints, *Mater. Manuf. Process.* **16** (2014) 305–311, doi: 10.1016/j.jmapro.2014.01.003.
30. V. Maduraimuthu, M. Vasudevan, V. Muthupandi, A. Bhaduri and T. Jayakumar, Effect of activated flux on the microstructure, mechanical properties and residual stresses of modified 9Cr–1Mo steel weld joints, *Metall. Mater. Trans. B, Process. Metall Mater. Process. Sci.* **43** (2012) 123–32, doi: 10.1007/s11663-011-9568-4.